

Article

Phase Composition, Hardness, and Thermal Shock Properties of AlCrTiN Hard Films with High Aluminum Content

Lijing Peng^{1,2} , Jun Zhang^{1,2} and Xiaoyang Wang^{1,2,*} ¹ College of Mechanical Engineering, Shenyang University, Shenyang 110044, China² Key Laboratory of Research and Application of Multiple Hard Films, Shenyang 110044, China

* Correspondence: wxy927@163.com

Abstract: TiCrAlN hard films based on TiN or CrN show superior properties in terms of hardness, wear resistance, and thermal stability due to the addition of alloying elements. AlCrTiN films based on AlN may have higher thermal shock properties, but the knowledge of AlCrTiN films with high Al content has been insufficient until now. In this study, two sets of AlCrTiN hard films with different Al contents of 48 at.% and 58 at.% among metal components were prepared via multi-arc ion plating so as to investigate the effect of Al content on the phase composition, hardness, and thermal shock resistance of the films. The same microstructures, morphologies, and thicknesses of the fabricated film samples were achieved by changing the combination of cathode alloy targets and adjusting the arc source current during deposition. The surface chemical composition, cross-sectional elemental distribution, microstructure, morphology, phase composition, surface hardness, film/substrate adhesion strength, and thermal shock performance of the AlCrTiN films were examined. The obtained results reveal that the two sets of AlTiCrN hard films are face-centered cubic solid solutions with a columnar fine grain structure and a preferred growth orientation of (200) crystal plane. The hardness of the AlCrTiN films can be improved up to HV2850 by properly reducing the Al content from 58 at.% to 48 at.%. Meanwhile, the film/substrate adhesion performance is strong enough in terms of critical loads greater than 200 N. Furthermore, the AlCrTiN films maintain high thermal shock resistance at 600 °C when the Al content decreases from 58 at.% to 48 at.%. The optimal composition of the AlCrTiN hard films is 25:13:15:47 (at.%), based on the consideration of hardness, adhesion, and thermal shock cycling resistance. This optimal AlCrTiN hard film can be suggested as an option for protective coatings of hot process die tools.



Citation: Peng, L.; Zhang, J.; Wang, X. Phase Composition, Hardness, and Thermal Shock Properties of AlCrTiN Hard Films with High Aluminum Content. *Coatings* **2023**, *13*, 547. <https://doi.org/10.3390/coatings13030547>

Academic Editor: Zsolt Czigan

Received: 1 February 2023

Revised: 25 February 2023

Accepted: 27 February 2023

Published: 3 March 2023



Copyright: © 2023 by the authors. Licensee MDPI, Basel, Switzerland. This article is an open access article distributed under the terms and conditions of the Creative Commons Attribution (CC BY) license (<https://creativecommons.org/licenses/by/4.0/>).

Keywords: AlCrTiN hard films; multi-arc ion plating; TiN/CrN molar ratio; hardness; phase composition; thermal shock cycle

1. Introduction

Nitride hard films have been extensively studied and developed for the application to cutting tools. In ternary nitride hard films, such as AlCrN, AlTiN, and CrTiN, the atomic substitution of metal components produces substitutional solid solution (M_xM_y)N nitride films, which cause lattice distortion and thus increase the film hardness. From the perspective of solid solution strengthening, when the crystal structure remains single phase without forming second phase, the larger the lattice distortion caused by the increase in the solute fraction, the more apparent the strengthening effect. Based on the stoichiometric chemical ratio of a (M_xM_y)N-type nitride film, the maximum solution strengthening hardness can be obtained at a molar ratio of the metal components close to 1:1 [1–3]. When accompanied by a crystal lattice distortion, the preferred crystal growth orientation and even phase composition of the film may also change [4,5].

To increase the hardness of TiN-based ternary nitride films and optimize their comprehensive properties, a third metal component is often added to form a quaternary substitutional ($Ti_xM_yM_z$)N nitride solid solution hard film. For example, TiAlCrN, TiAlZrN,

and TiAlNbN hard films generally exhibit high hardness and good comprehensive properties [6–11]. In consideration of the strong effect of Al on the oxidation resistance of Al-contained nitride hard films and the service requirements for nitride hard films as protective coatings of tools and molds, the thermal shock resistance of these films directly affects their actual utilization [12,13]. In fact, most studies on TiAlCrN hard films examined CrN-based and TiN-based films, while relatively few reports focused on AlCrTiN hard films with high Al contents.

Moreover, studies on AlCrN and AlTiN hard films with high Al content have shown that the AlN content up to 60–70 mol.% in $Ti_{1-x}Al_xN$ or $Cr_{1-x}Al_xN$ single solid solution phase with face-centred (fcc) cubic lattice can be retained without an occurrence of hexagonal close-packed (hcp) structure [14–16]. Additionally, the hardness of AlCrN and AlTiN hard films with fcc structure was generally larger than that with (hcp) structure. Similar results were also validated in the study of AlCrTiN hard films [8,17].

The present work aims to investigate the effects of Al content among metal components and Ti/Cr ratios on the phase composition, hardness, film/substrate adhesion strength, and thermal shock properties of AlCrTiN solid solution hard films with fcc structure. Through the deposition process design of multi-arc ion plating technology, different combinations of cathode arc source targets were selected, and the corresponding arc source current was adjusted to ensure the basic consistency of the fabricated film samples in terms of their surface morphology, cross-sectional morphology, N content distribution, and film thickness. Additionally, the deposition process was designed to ensure the Al contents among metal components in AlCrTiN hard films were less than 60 at.% so as to fabricate AlCrTiN solid solution hard films with fcc structure.

2. Materials and Methods

AlCrTiN hard films were prepared via multi-arc ion plating (MAD-4B) on high-speed steel (W18Cr4V, HRC63–64) substrates [18]. The co-deposition of AlCr and AlTi dual-arc source alloy targets (99.95% purity) with various compositions was performed to ensure the comparability of the deposited AlCrTiN hard films. The two arc source target currents were combined in different proportions to vary the film compositions, while other deposition parameters, such as the gas flow (pressure), deposition time, and deposition temperature, remained the same so as to ensure the basic consistency of the fabricated film samples in terms of their surface morphology, cross-sectional morphology, N content distribution, and film thickness. The coated samples were marked as 1#–6#, as shown in Table 1.

Table 1. Cathodic arc current combination during the deposition of AlTiCrN films (total current = 110–114 A).

Sample No.	Cathodic Arc Current (A)		Deposition Time (min)	Bias (V)
1	$Al_{70}Cr_{30}$	$Al_{70}Ti_{30}$	5 + 10 + 35	180
	56	54		
2	$Al_{70}Cr_{30}$	$Al_{50}Ti_{50}$	5 + 10 + 35	180
	58	55		
3	$Al_{50}Cr_{50}$	$Al_{64}Ti_{36}$	5 + 10 + 35	180
	59	55		
4	$Al_{70}Cr_{30}$	$Al_{50}Cr_{50}$	5 + 10 + 35	180
	50	60		
5	$Al_{50}Cr_{50}$	$Al_{64}Ti_{36}$	5 + 10 + 35	180
	55	55		
6	$Al_{50}Cr_{50}$	$Al_{64}Ti_{36}$	5 + 10 + 35	180
	58	52		

Double-target arc prebombardment was performed at a relatively high negative voltage bias (320–350 V) in an Ar atmosphere (3.0×10^{-1} Pa) for 10 min to clean the substrate and thus increase the film adhesion strength. The initial temperature of the arc bombardment process was 180 °C. After that, an alloy transition layer (deposition time: 5 min, bias voltage drop: –180 V), low N₂ flow film (deposition time: 10 min, bias voltage: –180 V), and normal N₂ flow film (deposition time: 35 min, bias voltage: –180 V) were obtained (Figure 1). The vacuum chamber temperature at the end of the entire deposition process was 200 ± 10 °C.

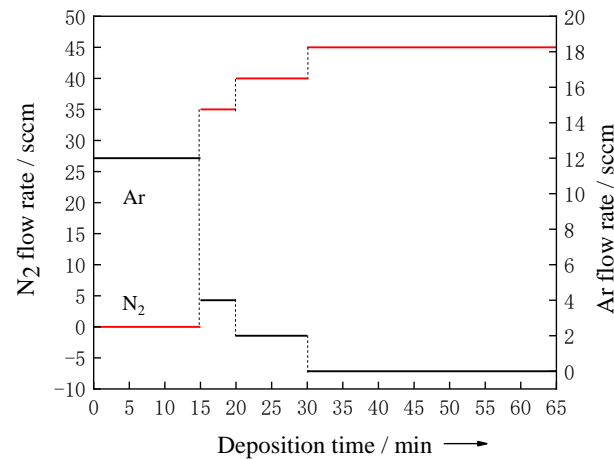


Figure 1. The flow rates of Ar and N₂ vs. deposition time. Black line: Ar, and red line: N₂.

Surface morphologies and compositions, cross-sectional morphologies, and elemental distributions of the as-deposited AlCrTiN films were observed with the aid of field-emission scanning electron microscopy (FE-SEM, S-4800) combined with energy-dispersive X-ray spectroscopy (EDS). Phase compositions of the as-deposited films were determined by X-ray diffraction (XRD, X'PertPRO) at a voltage of 40 kV, current of 40 mA, and wavelength (Cu-K α) of 0.154056 nm. The scanning angle (2θ) varied from 20° to 90° at a rate of 0.02°/min and step size of 0.05°. The obtained XRD data were analyzed by the Jade and Origin data processing software. The hardness of the as-deposited films was measured by performing Vickers micro-indentation tests (402 MVD). Three positions in the same field of view were tested at a load of 0.25 N for 20 s.

The film/substrate adhesion strengths of the prepared AlTiCrN films were determined by a WS-2005 automatic scratch tester. The maximum limit of the test load was 200 N, the loading rate was 200 N/min, the scratch speed was 4 mm/min, and the scratch length was 4 mm. A dynamic load method was used during testing, and an acoustic emission signal was recorded. The surface of each prepared sample film was examined by conducting 3–5 scratch tests.

Thermal shock tests were performed at 600 °C in a box-type electrical resistance furnace. A film sample was placed in the uniform temperature zone of the furnace for 10 min, quickly cooled to room temperature in water, and dried with hot air. The microstructure of the film layer was observed, and the test was repeated for 16 cycles.

3. Results and Discussion

3.1. Surface Morphology and Composition of AlCrTiN Hard Films

The surface morphologies of all the as-deposited films were observed by SEM. The surfaces of all coating layers were very similar and contain distributed “large particles” (liquid droplets). In general, each coating surface consisted of non-liquid and liquid droplets. These particles, with sizes below 6 μm , were formed from the micro-droplets sprayed from the cathode target surface [19,20]. Furthermore, the droplet densities on the surfaces of samples 1# and 4# were higher than those on the surfaces of other specimens,

which can be attributed to the higher arc currents and Al contents of the targets used for preparing these two samples. According to the literature, Al-Cr alloy targets are more likely to produce larger particles [21,22]. In addition, some scattered micro-pits were also observed on the film surfaces, owing to the shedding of loosely attached liquid particles during the deposition process (Figure 2).

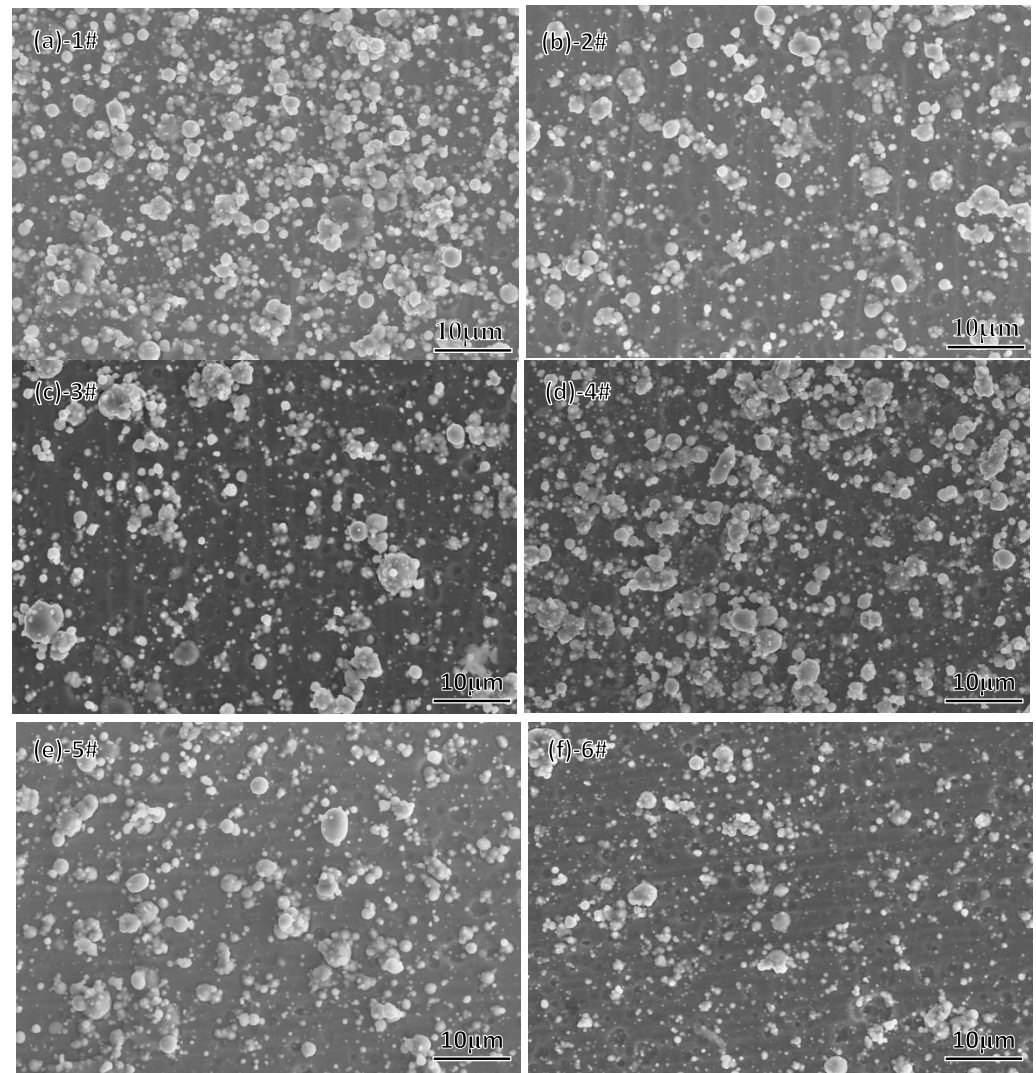


Figure 2. Surface morphologies of the deposited AlCrTiN films. The numbers (a–f) correspond to samples 1#–6#, respectively.

The surface compositions of the as-deposited films, including the droplet-free areas and large droplet particles, were determined by EDS. Because the N contents in the droplet-free areas of different film samples were nearly identical (46–47 at.%, see Figure 3a), the metal contents in the droplet-free areas could be normalized; then, an intuitive distribution triangle of the metal component contents could be established, as shown in Figure 3b. It was found that film samples 1#, 2#, 3#, and 4# exhibited almost the same Al content (58 at.%) and different Ti/Cr molar ratios, while the Al contents of samples 5# and 6# were equal to 48%. As a result, the AlCrTiN film samples with varied Al contents could be divided into two groups for the subsequent comparative study.

The droplet compositions on the film surfaces had relatively high uncertainties. Sample 3# is used as an example to illustrate this uncertainty. In the same field of view, the composition of droplet particles fluctuated significantly (Figure 4). This can be attributed to the following two reasons. First, it was closely related to the time of droplet attachment

to the film surface during deposition. Thus, the droplets that attached at the early stage of the deposition process formed a surface with a composition close to that of the droplet-free areas due to the subsequent deposition of the film layer [23]. However, almost all droplets attached at the later stage of the deposition process were metallic. Second, the compositions of the arc source targets strongly influenced the droplet composition. Because different droplets could overlap on the film surface, this also increased their compositional uncertainty.

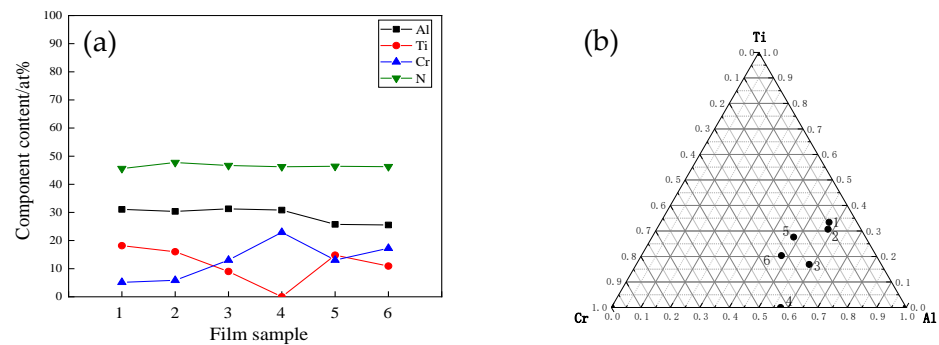


Figure 3. Chemical composition of the surface of the films. (a) Droplet-free film layer areas. (b) The corresponding normalized metal component contents.

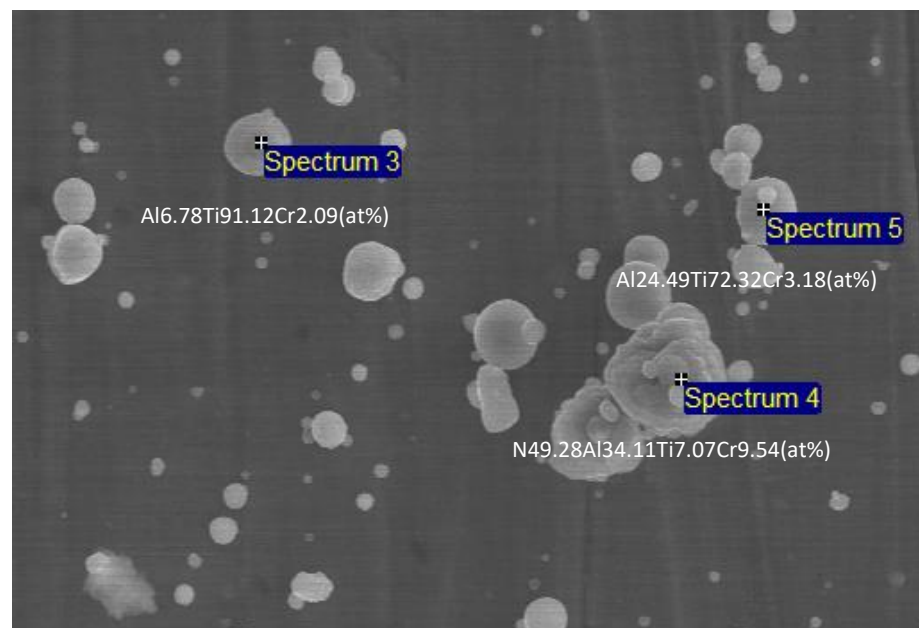


Figure 4. Chemical composition of the droplets on the surface of films.

3.2. Cross-Sectional Morphology and Elemental Distribution of AlCrTiN Hard Films

The brittle fracture cross-sectional SEM images of the as-deposited films obtained at room temperature are shown in Figure 5. The thicknesses of the films were very similar (2.1–2.3 μm) and all films exhibited dense and fine columnar crystal morphologies. Figure 6a–c present the grain growth morphology of the film surface in the droplet-free region of samples 5#, 6#, and 3#. Nearly the same fine grain growth morphology was observed in samples 1#–4#, and it was difficult to observe clear crystal grain boundaries. The possible reason is that film samples 1#–4# contained higher Al contents. In comparison, relatively clear grain boundaries were observed in samples 5# and 6#, and the grains of sample 6# were finer than those of sample 5#, with approximately half the grain cross-section size. The grain cross-section sizes of samples 1#–6# were between 30 nm and 60 nm and roughly consistent. The grain size of AlCrN films with an Al/Cr atomic

ratio from 1:1 to 2.3:1, deposited by the process parameters similar to those used in the present work, was reported as about 35 nm [24]. The fine columnar crystal microstructure of multi-component nitride hard films deposited by cathodic arc ion plating at a properly high bias is a characteristic of the deposition technology [25,26].

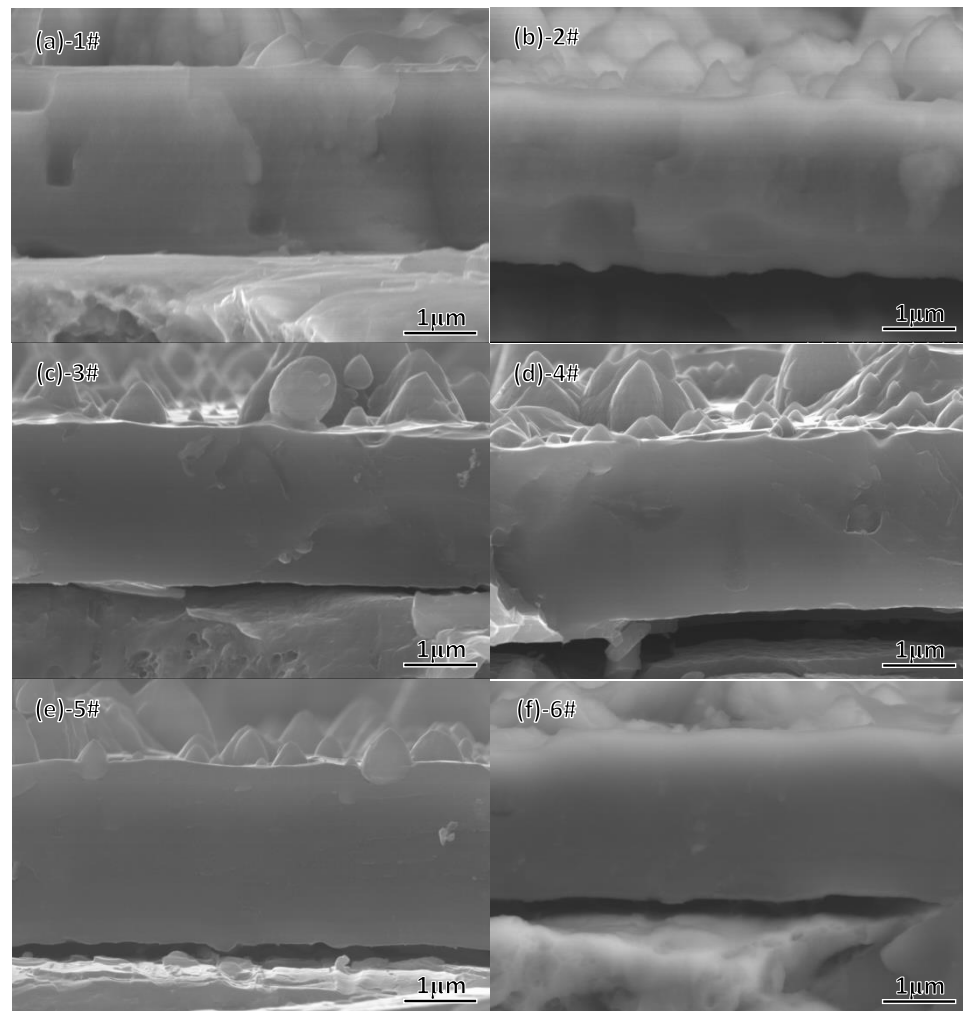


Figure 5. Cross-sectional morphologies of the films. The numbers (a–f) correspond to samples 1#–6#, respectively.

EDS line scanning was performed to determine the elemental distribution in the film growth direction. As expected, the sample coatings demonstrated similar distribution characteristics. The N content in each sample exhibited an apparent gradient in the film growth direction, while the contents of the other metal components remained almost unchanged (Figure 7).

Note that the utilized deposition technology and deposition process parameters produced different effects on the structure and properties of the multi-component nitride hard films. For example, the negative substrate bias affected the structure, composition, phase composition, and hardness of the films [27,28]. Meanwhile, the N₂ flow rate and substrate temperature influenced the N content, structure, and hardness of the film layer [29,30]. Although the compositions of the films prepared using different deposition technologies and conditions were either the same or very similar, the properties of these films differed considerably [31,32].

During deposition, the sum of the two arc currents was maintained constant at 110–114 A, and the deposition time was 5 + 10 + 35 min. Meanwhile, the negative bias voltage of the substrate as well as the argon and nitrogen flow rates at the corresponding

stages of the deposition process were the same for all film samples. This ensured the nearly identical distributions of N atoms, microstructures, and thicknesses of all films; therefore, the prepared samples mainly differed in their compositions, and their phase compositions were determined by the corresponding film compositions. Finally, the film and phase compositions synergistically influenced the film performance. In summary, film composition was a single important factor affecting film characteristics, which allowed for the examination of the influences of Al content and Ti/Cr molar ratio on the phase composition, hardness, film/substrate bonding strength, and thermal shock properties of the fabricated AlCrTiN hard films.

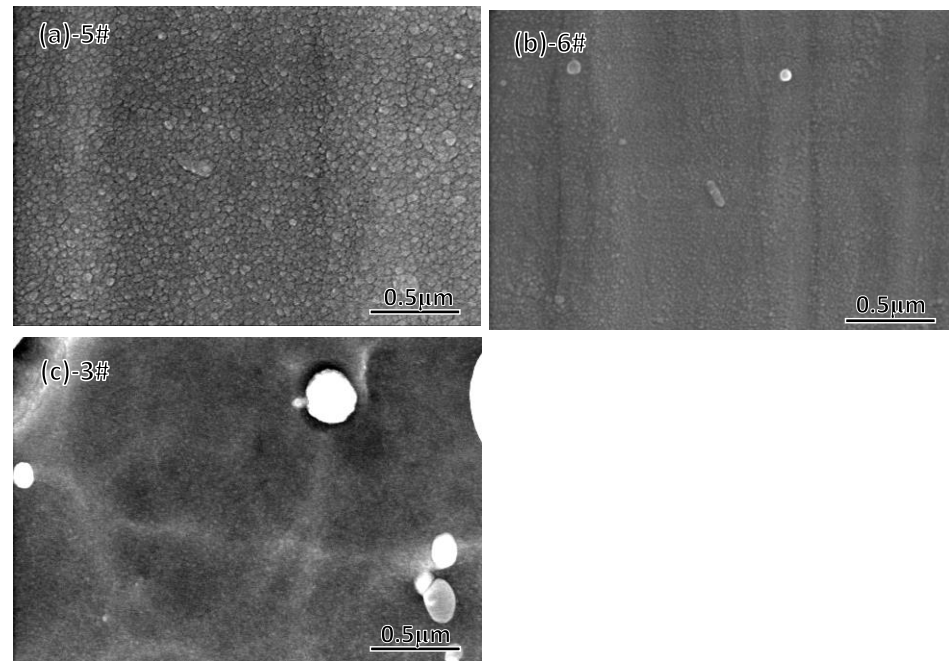


Figure 6. The grain growth morphology of the film surface in the non-droplet region; (a–c) correspond to samples 5#, 6#, and 3#, respectively.

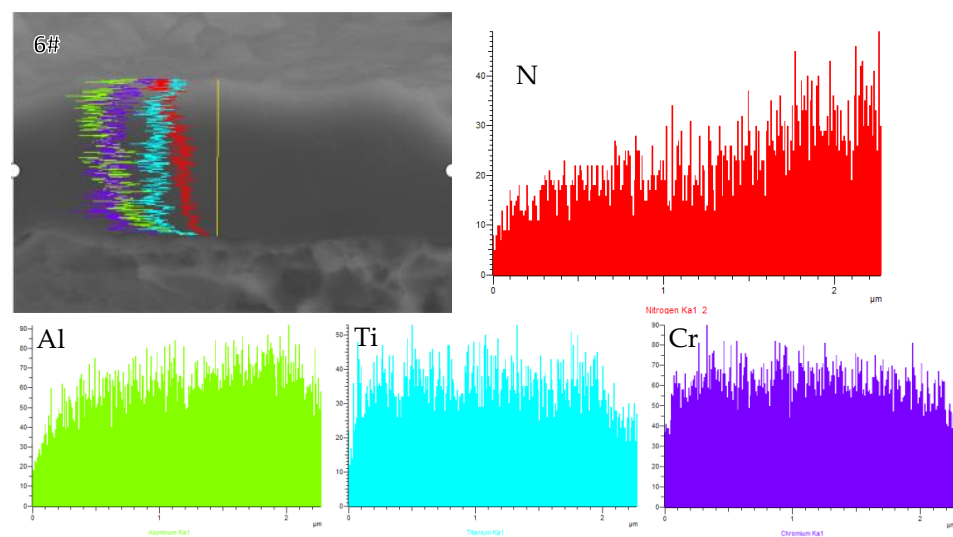


Figure 7. Cross-sectional elemental distribution in the growth direction of the films (sample 6#).

3.3. Phase Compositions of AlCrTiN Hard Films

All films were investigated by small-angle XRD, and the obtained results were analyzed by the JADE software. The XRD patterns depicted in Figure 8a,b exhibit similar char-

acteristics in diffraction peak intensity distribution. According to the standard diffraction patterns of CrN and TiN (Figure 9a,b), the prepared AlCrTiN films are mainly composed of the face-centered cubic (fcc) AlCrTiN phase with substitutional solid solution characteristics and the preferred growth orientation of the (200) crystal plane (tagged with the solid circle symbol, in Figure 8a). Additionally, a TiAlCr alloy phase (tagged with the diamond symbol, in Figure 8a) with varied metal element concentrations, resulting from the droplets attached at the later stage of the deposition process, can be identified. Notably, the fcc AlCrTiN phase present in films 3#, 4#, and 6# exhibits a diffraction peak smoothing or separation feature (Figure 8b) due to the high Al and Cr contents [15,16]. However, unlike the phase transition tendency from fcc structure to hcp structure in $Ti_{1-x}Al_xN$ or $Cr_{1-x}Al_xN$ films as the Al content among metal components increases up to 60–70 mol.%, the fcc structure rather than hcp structure seems easily retained for AlN in the AlTiCrN films. This may be attributed to the fact that complex lattice distortion due to the addition of Ti atoms into AlCrN lattice weakens the driving force to form hcp structure of AlN phase, as shown by the XRD patterns of films 2# and 5#.

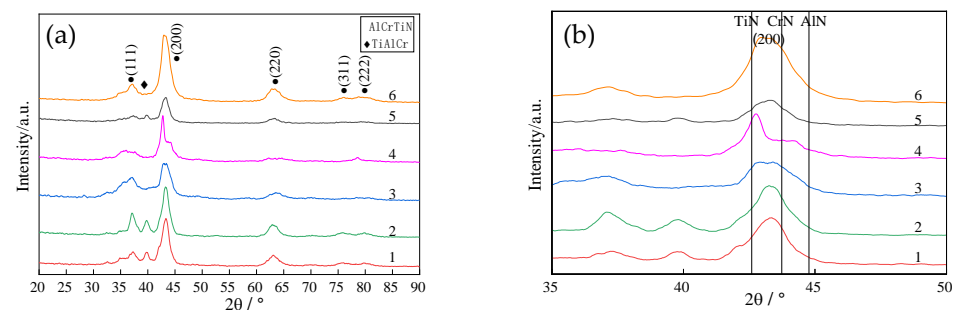


Figure 8. (a) XRD patterns of AlCrTiN films, (b) Partial enlarged detail of the XRD patterns.

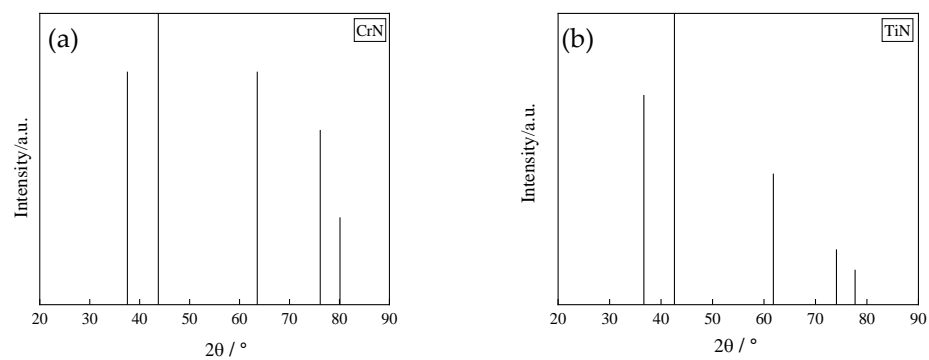


Figure 9. Standard XRD patterns of CrN and TiN. (a) CrN. (b) TiN.

The (200) crystal plane diffraction peak of film sample 4# corresponds to the Al(Cr)N fcc phase with high Al content and Cr(Al)N fcc phase with high Cr content. The Ti contents of samples 3# and 6# are similar, and these samples also exhibit high Al and Cr concentrations, indicating a separation trend. However, their Cr(Al) contents are lower than those of sample 4# because some Cr(Al) atoms are substituted by Ti atoms, which weaken the separation trend. This resulted in the formation of a single AlCrTiN phase broadening the (200) diffraction peak. Therefore, no isolated TiN, CrN, or AlN phases are present in the prepared films except for in sample 4#.

From the results obtained for samples 4#, 3#, 2#, and 1# with the same Al contents, it can be concluded that increasing the Ti/Cr ratio promotes the formation of a single fcc solid solution. The same feature was observed for samples 5# and 6#, suggesting that the AlCrTiN film easily maintains the fcc structure even at high Al contents close to 60%. Although the Al contents in all films (except for sample 4#) are as high as 48%–58%, their diffraction peaks remain between the standard diffraction peaks of the TiN and CrN phases,

indicating that the peaks of the (200) crystal plane obtained for these films are shifted to smaller angles.

As shown in Figure 3b, the AlCrTiN film can be seen to be a substitutional solid solution formed by the TiN, CrN, and AlN phases, and their respective proportions are replaced by the normalized proportions of metal element concentrations. The ideal lattice constants of the fcc solid solution of each group of the fabricated film samples were calculated according to Vegard's law. Additionally, considering the characteristic diffraction peak position of the (200) crystal plane of the AlCrTiN film, the lattice constant of the fcc (AlCrTi)N solid solution phase was directly determined using the JADE software. The obtained results are shown in Figure 10. The experimentally measured lattice constants of all films (except for sample 4#) are significantly higher than the values calculated by Vegard's law because TiN, CrN, and AlN form a complex fcc solid solution, resulting in large lattice distortions and the formation of vacancy defects. Because the conducted film deposition was a non-equilibrium process, point defects and residual thermal stress were generated in the films, increasing the lattice constant [33].

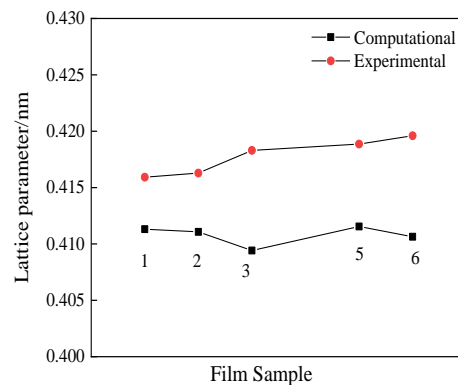


Figure 10. Lattice constant of the films obtained from the experiments and calculations using Vegard's law. Notes: 1. excluding film 4#; 2. the 2θ angle of (200) crystal plane of films 3# and 6# is an estimated value.

The texture characteristics of a multi-component nitride film are strongly related to the utilized deposition technology and process parameters. The $\text{Cr}_{1-x}\text{Al}_x\text{N}$ film prepared by multi-arc ion plating technology, which is similar to the fabrication method used in the present study, exhibited similar properties (a B1-NaCl-type fcc structure was formed below $x = 0.6$, and its preferred growth orientations corresponded to the (200) and (111) crystal planes) [34]. However, the $\text{Al}_x\text{Cr}_{1-x}\text{N}$ film produced by unbalanced magnetron sputtering with two sputtering sources at $0.31 \leq x \leq 0.71$ had a preferred orientation of the single (111) crystal plane [35].

In this work, the single composition change did not change the phase composition or crystal structure of the AlCrTiN films, owing to the consistency of the deposition process. All films (except for 4#) were composed of the single AlCrTiN substitution fcc solid solution phase and had the same preferred growth orientation corresponding to the (200) crystal plane. Therefore, it can be concluded that the performance difference of these films originated from composition changes. This effect mainly involved solution strengthening caused by lattice distortion.

3.4. Hardness and Adhesion of AlCrTiN Hard Films

The microhardness test data obtained for all film layers of droplet-free areas are listed in Table 2. It shows that the hardness values of AlCrTiN samples 1#–4# with equal molar ratios of AlN (~58%) are lower than those of the AlCrN and AlTiN films with the same AlN molar ratio [16,35]. These results indicate that the hardness of the AlCrTiN films formed by adding Ti or Cr atoms to AlCrN or AlTiN films with high Al contents is relatively low.

However, with a decrease in the molar ratio of AlN to 48%, the hardness values of the AlCrTiN films 5# and 6# increase as compared with those of films 2# and 3#.

Table 2. The microhardness of AlCrTiN films.

Sample No.	AlN/mol %	TiN/mol %	CrN/mol %	TiN/CrN	Microhardness (HV)	Adhesion (N)
1	57.14	33.39	9.44	3.54	2680 ± 200	>150
2	58.14	30.67	11.2	2.74	2650 ± 200	>200
3	58.67	16.88	24.47	0.69	2620 ± 200	>200
4	57.40	0	42.6	0	2750 ± 200	>130
5	48.06	27.6	24.36	1.13	2850 ± 200	>200
6	47.54	20.33	32.13	0.63	2730 ± 200	>200

Under the premise of maintaining the fcc structure of a ternary substitutional solid solution nitride film (such as AlCrN, TiAlN, and TiCrN), as the content of the second metal component increases, the lattice distortion will increase, and then the hardness of the film layer tends to increase [3,34,36]. The hardness maximum value is reached when the metal component ratio is close to 1:1.

The present AlTiCrN substitutional solid solution films were formed by adding Ti atoms to AlCrN fcc structure and replacing some of the Al and Cr atoms because the ratio of N/Metal is the same and almost equal to 1:1. In this case, three solid solution combinations were produced: a combination of AlN and TiN, a combination of AlN and CrN (both of which have high AlN fractions), and a combination of TiN and CrN. Therefore, the hardness of the AlTiCrN solid solution film was reduced because the AlCrN and AlTiN films with high Al contents exhibited low hardness values. Only when the addition of Ti atoms reached a certain fraction among the metal components and the AlTiCrN solid solution was gradually transformed into a combination of AlN/TiN and AlN/CrN, both with a small concentration difference, did the film hardness increase, as shown by films 5# and 6#.

According to previous studies, the hardness of the $\text{Cr}_{0.66}\text{Al}_{0.34}\text{N}$ ternary film is 28.5 GPa. With the addition of the Ti component at $f_{\text{Ti}} = 5\%$ and 10% , the hardness values of the resulting $\text{Cr}_{65}\text{Ti}_5\text{Al}_{30}\text{N}$ and $\text{Cr}_{61}\text{Ti}_{10}\text{Al}_{29}\text{N}$ films increase to 34 and 40 GPa, respectively. When f_{Ti} is further increased, the hardness begins to decrease slowly. When the Ti content reaches 64%, the hardness of the $\text{Cr}_{26}\text{Ti}_{64}\text{Al}_{10}\text{N}$ film decreases to 29 GPa [37]. However, the hardness of the $\text{Ti}_{0.17}\text{Al}_{0.53}\text{Cr}_{0.30}\text{N}$, $\text{Ti}_{0.23}\text{Al}_{0.36}\text{Cr}_{0.4}\text{N}$, and $\text{Ti}_{0.46}\text{Al}_{0.20}\text{Cr}_{0.34}\text{N}$ films prepared using different combinations of the TiAl, Cr, and Al targets monotonically increases with a decrease in the Al content and increase in the Ti content [17]. The work to investigate the effect of bias on the composition and hardness of TiAlCrN films shows that as the bias increases from 100 V, 150 V, 200 V to 250 V, the composition of the films is successively changed into $\text{Ti}_{23}\text{Al}_{18}\text{Cr}_{20}\text{N}$, $\text{Ti}_{27}\text{Al}_{16}\text{Cr}_{21}\text{N}$, $\text{Ti}_{20}\text{Al}_{14}\text{Cr}_{29}\text{N}$, $\text{Ti}_{23}\text{Al}_{12}\text{Cr}_{31}\text{N}$, and the hardness is successively changed into HV2800, HV5100, HV4650, HV4650V [38]. Thus, it can be concluded that the hardness values of the TiN-based TiAlCrN and CrN-based CrTiAlN films are generally higher than that of the AlN-based AlTiCrN film.

In addition, the N/metal ratio of nitride hard films directly affects their hardness, which decreases when this ratio deviates significantly from the stoichiometric ratio of 1:1 [39,40]. Therefore, the N content in the hardening film layer is generally maintained between 45 and 52 at.%, which is close to the ideal chemical ratio required to maximize the hardness of the nitride film. The N contents in the hardening surface layers of the as-deposited AlTiCrN solid solution films prepared in this study amounted to 47%–48%, which ensured their maximum hardness at various ratios of the metal components.

The film/substrate adhesive strength values of the AlCrTiN hard films (Table 2) suggest that the adhesion between the film and substrate is relatively strong, except for film samples 1# and 4# (the other films layers withstood critical loads exceeding 200 N). Previous studies have shown that designing the N gradient distribution in nitride hard films is an effective method for improving the film/substrate adhesion performance [41,42]. For example, the

adhesive strength of a (TiAlNb)N film with N gradient distribution prepared was much larger than that of a (TiAlNb)N film without an alloy transition layer and N gradient distribution [11,43].

In the present study, the ion bombardment of the high-speed steel substrate prior to film deposition and subsequent deposition of the alloy transition layer prevented the separation of the film from the substrate and increased the film adhesive strength. Optimizing the gradient distribution of the N element in the film growth direction inhibits the accumulation of growth stress and produces a gradient of the thermal expansion coefficient, which helps improve both the adhesion [41,42] and thermal shock performance of the film.

3.5. Thermal Shock Cycling Performance of AlCrTiN Hard Films

The cutting tools and dies coated with nitride hard films are generally required to have long service lives and good machining properties under hot and cold cycling conditions. Therefore, the corresponding hard films must possess high thermal shock resistances.

The fabricated AlCrTiN hard films were subjected to thermal shock cycles at 600 °C, and the changes in the surface morphology were observed after each cycle. After eight cycles, no significant changes in the film surfaces were detected by SEM with a 2000× magnification. The surface changes of two samples, 1# with more droplets and 5# with fewer droplets, are given as examples, as shown in Figure 11. To observe the film surface more carefully, the magnification was increased to 10,000×. During the entire eight thermal shock cycles, the observable change in the surface morphology was that the surface of droplet particles became coarse, and some very small particles appeared. In contrast, negligible morphological changes occurred in the droplet-free areas. This indicates that the surface oxidation rate of the droplets was significantly higher than that of the droplet-free area. After the eighth cycle, neither cracking or shedding of droplets nor cracks on the surface of the droplet-free area were detected in any of the samples. Figure 12a,b show the surface changes of samples 2# and 3#, respectively.

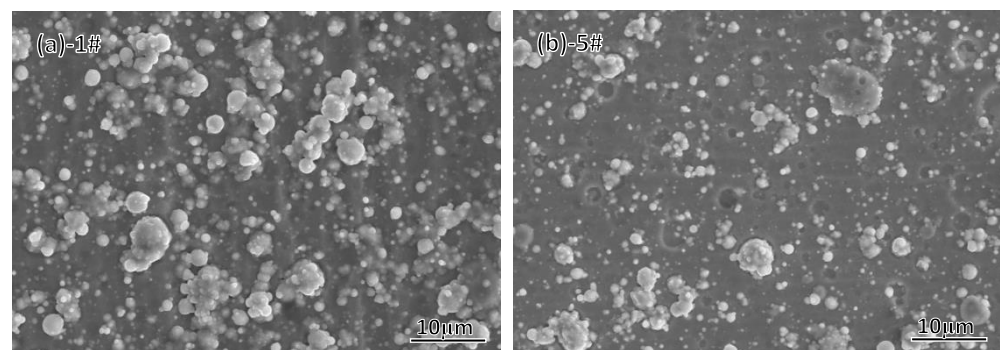


Figure 11. Surface morphologies of AlTiCrN hard films after the 8th thermal shock cycle. (a) Sample 1#. (b) Sample 5#.

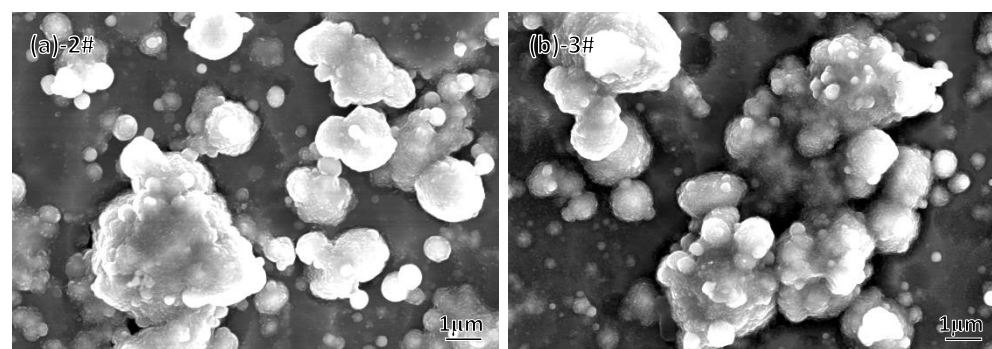


Figure 12. Surface morphologies of film samples 2# and 3# after 8th thermal shock cycle. (a) Sample 2#. (b) Sample 3#.

After the 16th cycle, inconsistent changes were observed on the film surfaces with different compositions (Figure 13). For films 1# and 4#, no obvious changes in the film surface morphologies (the droplet-free areas) were observed, as shown by the red circle in Figure 13a,d. However, a few of cracks formed on the surfaces of droplet particles. For films 2# and 3#, the obvious growth of the cross-section grain size of the film layer (the droplet-free areas) was observed up to about 200 nm and 300 nm, respectively, as shown by the red circle in Figure 13b,c. Meanwhile, a few cracks were observed on droplet particles. For films 5# and 6#, on the film surface of the droplet-free areas, the grain boundaries became blurred and the cross-section size of grain in film 5# seemed to be larger than that in film 6#, as shown by the red circle in Figure 13e,f. Additionally, no visible cracks formed on the surfaces of droplet particles. In general, all films exhibited no cracks in the droplet-free area through 16 thermal shock cycles. This means that the prepared film samples possessed high thermal shock resistances.

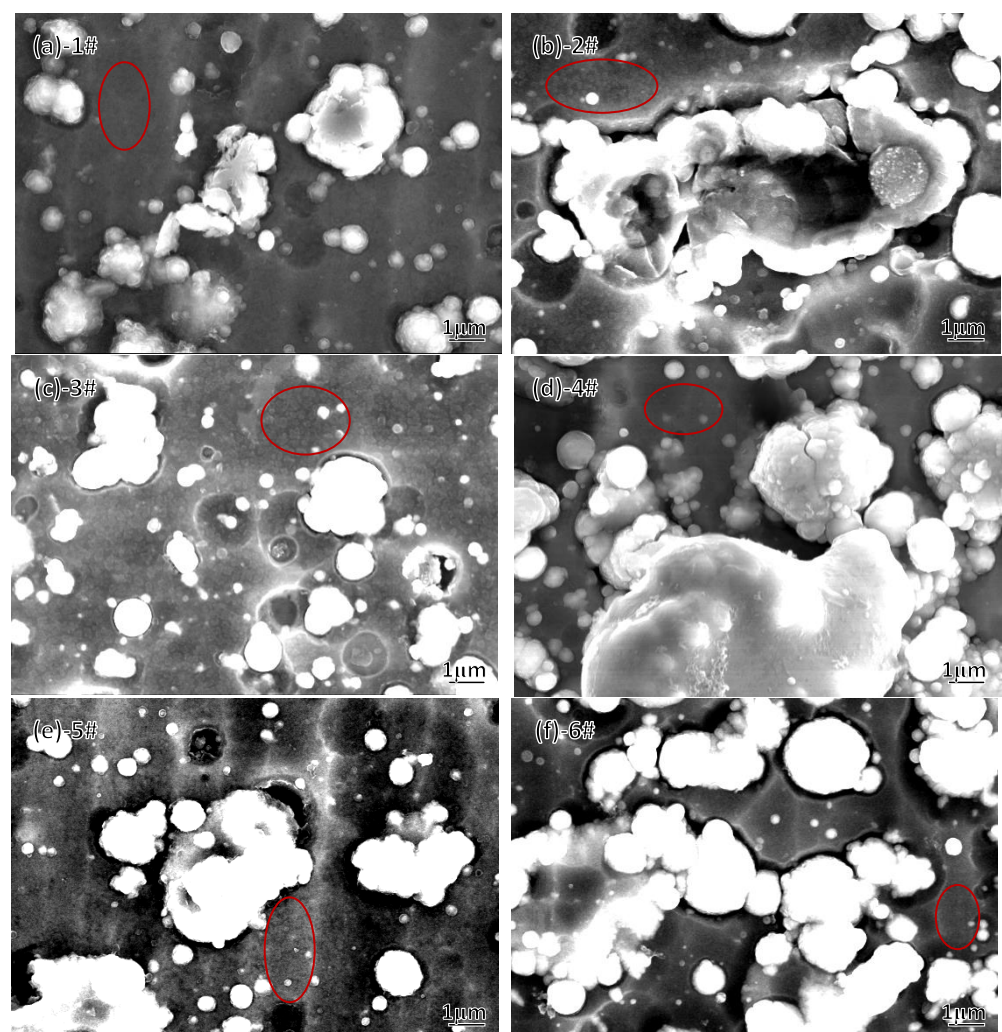


Figure 13. Surface morphologies of film samples after 16 thermal shock cycles. The numbers (a–f) correspond to sample numbers 1#–6#, respectively. Red circle region: droplet-free area.

The Al element has a relatively high oxidation resistance because it easily forms a dense oxide (Al_2O_3) layer that covers the film surface during thermal shock, thus preventing oxygen atoms from further penetrating the film and resulting in the oxidation of the film layer [44]. However, the Cr element can promote the oxidation of Al atoms and accelerate the formation of Al_2O_3 [45]. Therefore, a film with high Al content typically exhibits high thermal shock resistance. In the present study, all film layers of the droplet-free areas with high Al and Cr contents demonstrated high thermal shock resistance. Because the

thermal shock cycling temperature was 600 °C, which is lower than the preferred oxidation temperature of Al [46–48], films 1#–4# with higher Al contents, in comparison with films 5# and 6#, did not exhibit obvious advantages in terms of thermal shock resistance.

4. Conclusions

In this study, two sets of AlCrTiN hard films with different Al contents among metal components were prepared. All of the films exhibited almost identical surface morphologies, cross-sectional microstructures and morphologies, thicknesses, and N content distributions because the combination of alloy targets and parameters of the deposition process were adjusted for each sample. The main conclusions from the obtained results are summarized below.

1. All AlTiCrN hard films (i.e., droplet-free areas, the same below) consist of the fcc solid solutions with a columnar fine microstructure and the preferred growth orientation of (200) crystal plane at high Al contents from 48 up to 58 at.%. AlCrTiN films easily maintains the fcc structure even at high Al contents up to 58 at.% due to the complex lattice distortion.
2. The hardness of AlTiCrN films with an Al content of 58 at.% is significantly lower than those of TiCrAlN and CrTiAlN hard films with high Ti and Cr contents, and varying the Ti/Cr ratio does not increase hardness of the AlTiCrN films.
3. The hardness of AlCrTiN films can be improved up to HV2850 by properly reducing the Al content from 58 at.% to 48 at.%. Meanwhile, the film/substrate adhesion performance is strong enough in terms of critical loads greater than 200 N.
4. AlCrTiN films maintain high thermal shock resistance at 600 °C even when the Al content decreases from 58 at.% to 48 at.%. In the droplet-free area of the film surface, no crack appeared through 16 thermal shock cycles. The thermal shock failure of the films is typically manifested as a rupture and droplet particles falling off.
5. The optimal composition of AlCrTiN hard films is 25:13:15:47 (at.%), which is determined from the results of hardness, adhesion, and thermal shock cycling resistance measurements. This optimal AlCrTiN hard film can be used as an option for protective coatings of hot-pressure die tools.

Author Contributions: Conceptualization, methodology, J.Z.; investigation, L.P.; resources, X.W.; data curation, writing—original draft preparation, L.P.; writing—review and editing, X.W.; funding acquisition, X.W. All authors have read and agreed to the published version of the manuscript.

Funding: This research was funded by Liaoning Province Doctor Start-up Fund, grant number 2021-BS-276.

Institutional Review Board Statement: Not applicable.

Informed Consent Statement: Not applicable.

Data Availability Statement: Not applicable.

Conflicts of Interest: The authors declare no conflict of interest.

References

1. Hörling, A.; Hultman, L.; Odén, M.; Sjöln, J.; Karlsson, L. Mechanical properties and machining performance of $Ti_{1-x}Al_xN$ -coated cutting tools. *Surf. Coat. Technol.* **2004**, *191*, 384–392. [[CrossRef](#)]
2. Lamni, R.; Sanjinés, R.; Parlinska-Wojtan, M.; Karimi, A.; Lévy, F. Microstructure and nanohardness properties of Zr-Al-N and Zr-Cr-N thin films. *J. Vac. Sci. Technol. A* **2005**, *23*, 593–598. [[CrossRef](#)]
3. Niu, E.W.; Li, L.; Lv, G.H.; Chen, H.; Li, X.Z.; Yang, X.Z.; Yang, S.Z. Characterization of Ti-Zr-N films deposited by cathodic vacuum arc with different substrate bias. *Appl. Surf. Sci.* **2008**, *254*, 3909–3914. [[CrossRef](#)]
4. Falub, C.V.; Karimi, A.; Ante, M.; Kalss, W. Interdependence between stress and texture in arc evaporated Ti-Al-N thin films. *Surf. Coat. Technol.* **2007**, *201*, 5891–5898. [[CrossRef](#)]
5. Kimura, A.; Hasegawa, H.; Yamada, K.; Suzuki, T. Metastable $Ti_{1-x}Al_xN$ films with different Al content. *J. Mater. Sci. Lett.* **2000**, *19*, 601–602. [[CrossRef](#)]

6. Donohue, L.A.; Cawley, J.; Brooks, J.S.; Münz, W.D. Deposition and characterization of TiAlZrN films produced by a combined steered arc and unbalanced magnetron sputtering technique. *Surf. Coat. Technol.* **1995**, *74*, 123–134. [[CrossRef](#)]
7. Zhang, J.; Guo, W.; Zhang, Y.; Guo, Q.; Wang, C.; Zhang, L. Mechanical properties and phase structure of (TiAlZr)N films deposited by multi arc ion plating. *Thin Solid Film.* **2009**, *517*, 4830–4834. [[CrossRef](#)]
8. Yamamoto, K.; Sato, T.; Takahara, K.; Hanaguri, K. Properties of (Ti,Cr,Al)N coatings with high Al content deposited by new plasma enhanced arc-cathode. *Surf. Coat. Technol.* **2003**, *174*, 620–626. [[CrossRef](#)]
9. Santana, A.E.; Karimi, A.; Derflinger, V.H.; Schütze, A. Microstructure and mechanical behavior of TiAlCrN multilayer thin films. *Surf. Coat. Technol.* **2003**, *177*, 334–340. [[CrossRef](#)]
10. Hsu, C.H.; Chen, K.L.; Lin, Z.H.; Su, C.Y.; Lin, C.K. Bias effects on the tribological behavior of cathodic arc evaporated CrTiAlN coatings on AISI 304 stainless steel. *Thin Solid Film.* **2010**, *518*, 3825–3829. [[CrossRef](#)]
11. Zhang, J.; Yin, L.Y. Microstructure and mechanical properties of (Ti,Al,Nb)N hard films with N-gradient distributions. *Thin Solid Film.* **2015**, *584*, 141–145. [[CrossRef](#)]
12. PalDey, S.; Deevi, S.C. Single layer and multilayer wear resistant coatings of (Ti,Al)N: A review. *Mater. Sci. Eng. A* **2003**, *342*, 58–79. [[CrossRef](#)]
13. Greczynski, G.; Hultman, L.; Odén, M. X-ray photoelectron spectroscopy studies of $Ti_{1-x}Al_xN$ ($0 \leq x \leq 0.83$) high temperature oxidation: The crucial role of Al concentration. *Surf. Coat. Technol.* **2019**, *374*, 923–934. [[CrossRef](#)]
14. Pemmasani, S.P.; Valleti, K.; Gundakaram, R.C.; Rajulapati, K.V.; Mantripragada, R.; Koppoju, S.; Joshi, S.V. Effect of microstructure and phase constitution on mechanical properties of $Ti_{1-x}Al_xN$ coatings. *Appl. Surf. Sci.* **2014**, *313*, 936–946. [[CrossRef](#)]
15. Wang, D.; Lin, S.S.; Liu, L.Y.; Xue, Y.N.; Yang, H.Z.; Jiang, B.L.; Zhou, K.S. Effect of Bias Voltage on Microstructure and Erosion Resistance of CrAlN Coatings Deposited by Arc Ion Plating. *Rare Met. Mater. Eng.* **2020**, *49*, 2583–2590.
16. Hasegawa, H.; Suzuki, T. Effects of second metal contents on microstructure and micro-hardness of ternary nitride films synthesized by cathodic arc method. *Surf. Coat. Technol.* **2004**, *188–189*, 234–240. [[CrossRef](#)]
17. Vattanaprteep, N.; Panich, N.; Surinphong, S.; Tungasmita, S.; Wangyao, P. Structural and Mechanical Properties of Nanostructured TiAlCrN Thin Films Deposited by Cathodic Arc Deposition. *High Temp. Mater. Proc.* **2013**, *32*, 107–111. [[CrossRef](#)]
18. Zhang, J.; Peng, L.; Wang, X.; Liu, D.; Wang, N. Effects of Zr/(Zr+Ti) Molar Ratio on the Phase Structure and Hardness of $Ti_xZr_{1-x}N$ Films. *Coatings* **2021**, *11*, 1342. [[CrossRef](#)]
19. Harris, S.G.; Doyle, E.D.; Wong, Y.C.; Munroe, P.R.; Cairney, J.M.; Long, J.M. Reducing the macroparticle content of cathodic arc evaporated TiN coatings. *Surf. Coat. Technol.* **2003**, *183*, 283–294. [[CrossRef](#)]
20. Shiao, M.H.; Shieu, F.S. Formation of macroparticles in arc ion-plated nitride coatings. *J. Vac. Sci. Technol. A Vac. Surf. Film.* **2001**, *19*, 703–705. [[CrossRef](#)]
21. Wan, X.S.; Zhao, S.S.; Yang, Y.; Gong, J.; Sun, C. Effects of nitrogen pressure and pulse bias voltage on the properties of Cr-N coatings deposited by arc ion plating. *Surf. Coat. Technol.* **2009**, *204*, 1800–1810. [[CrossRef](#)]
22. Vyskoceil, J.; Musil, J. Cathodic arc evaporation in thin film technology. *Vac. Sci. Technol.* **1992**, *A10*, 1740–1748. [[CrossRef](#)]
23. Shiao, M.H.; Shieu, F.S. A formation mechanism for the macroparticles in arc ion-plated TiN films. *Thin Solid Films* **2001**, *386*, 27–31. [[CrossRef](#)]
24. Tritremmel, C.; Daniel, R.; Lechthaler, M.; Polcik, P.; Mitterer, C. Influence of Al and Si content on structure and mechanical properties of arc evaporated Al-Cr-Si-N thin films. *Thin Solid Film.* **2013**, *534*, 403–409. [[CrossRef](#)]
25. Kuczyk, M.; Krülle, T.; Zawischa, M.; Kaspar, J.; Zimmer, O.; Leonhardt, M.; Leyens, C.; Zimmermann, M. Microstructure and mechanical properties of high entropy alloy nitride coatings deposited via direct current cathodic vacuum arc deposition. *Surf. Coat. Technol.* **2022**, *448*, 128916–128930. [[CrossRef](#)]
26. Chen, W.L.; Zheng, J.; Lin, Y.; Kwon, S.; Zhang, S.L. Comparison of AlCrN and AlCrTiSiN coatings deposited on the surface of plasma nitrocarburized high carbon steels. *Appl. Surf. Sci.* **2015**, *332*, 525–532. [[CrossRef](#)]
27. Cai, F.; Chen, M.; Li, M.; Zhang, S. Influence of negative bias voltage on microstructure and property of Al-Ti-N films deposited by multi-arc ion plating. *Ceram. Int.* **2017**, *43*, 3774–3783. [[CrossRef](#)]
28. Liu, W.; Li, A.; Wu, H.; He, R.; Huang, J.; Long, Y.; Deng, X.; Wang, Q.; Wang, C.; Wu, S. Effects of bias voltage on microstructure, mechanical properties, and wear mechanism of novel quaternary (Ti, Al, Zr)N coating on the surface of silicon nitride ceramic cutting tool. *Ceram. Int.* **2016**, *42*, 17693–17697. [[CrossRef](#)]
29. Tang, J.F.; Lin, C.Y.; Yang, F.C.; Chang, C.L. Influence of Nitrogen Content and Bias Voltage on Residual Stress and the Tribological and Mechanical Properties of CrAlN Films. *Coatings* **2020**, *10*, 546. [[CrossRef](#)]
30. Larijani, M.M.; Tabrizi, N.; Norouzian, S.; Jafari, A.; Lahouti, S.; Hosseini, H.H.; Afshari, N. Structural and mechanical properties of ZrN films prepared by ion beam sputtering with varying N_2/Ar ratio and substrate temperature. *Vacuum* **2006**, *81*, 550–555. [[CrossRef](#)]
31. Donohue, L.A.; Cawley, J.; Brooks, J.S. Deposition and characterisation of arc-bond sputter Ti_xZr_yN coatings from pure metallic and segmented targets. *Surf. Coat. Technol.* **1995**, *72*, 128–138. [[CrossRef](#)]
32. Le Bourhis, E.; Goudeau, P.; Staia, M.H.; Carrasquero, E.; Puchi-Cabrera, E.S. Mechanical properties of hard AlCrN-based coated substrates. *Surf. Coat. Technol.* **2009**, *203*, 2961–2968. [[CrossRef](#)]
33. Elstner, F.; Gautier, C.; Moussaoui, H.; Piot, O.; Machet, J. A comparative study of structure and residual stress in chromium nitride films deposited by vacuum arc evaporation, ion plating, and DC magnetron sputtering. *Phys. Stat. Sol.* **2010**, *158*, 505–521. [[CrossRef](#)]

34. Hasegawa, H.; Kawate, M.; Suzuki, T. Effects of Al contents on microstructures of $\text{Cr}_{1-x}\text{Al}_x\text{N}$ and $\text{Zr}_{1-x}\text{Al}_x\text{N}$ films synthesized by cathodic arc method. *Surf. Coat. Technol.* **2005**, *200*, 2409–2413. [[CrossRef](#)]
35. Kim, G.S.; Lee, S.Y. Microstructure and mechanical properties of AlCrN films deposited by CFUBMS. *Surf. Coat. Technol.* **2006**, *201*, 4361–4366. [[CrossRef](#)]
36. Boxman, R.L.; Zhitomirsky, V.N.; Grimberg, I.; Rapoport, L.; Goldsmith, S.; Weiss, B.Z. Structure and hardness of vacuum arc deposited multi-component nitride coatings of Ti, Zr and Nb. *Surf. Coat. Technol.* **2000**, *125*, 257–262. [[CrossRef](#)]
37. Lin, J.; Zhang, X.; Ou, Y.; Wei, R. The structure, oxidation resistance, mechanical and tribological properties of CrTiAlN coatings. *Surf. Coat. Technol.* **2015**, *277*, 58–66. [[CrossRef](#)]
38. Zhang, J.; Lv, H.; Cui, G.; Jing, Z.; Wang, C. Effects of bias voltage on the microstructure and mechanical properties of (Ti,Al,Cr)N hard films with N-gradient distributions. *Thin Solid Film.* **2011**, *519*, 4818–4823. [[CrossRef](#)]
39. Tay, B.K.; Shi, X.; Yang, H.S.; Tan, H.S.; Chua, D.; Teo, S.Y. The effect of deposition conditions on the properties of TiN thin films prepared by filtered cathodic vacuum-arc technique. *Surf. Coat. Technol.* **1999**, *111*, 229–233. [[CrossRef](#)]
40. Sundgren, J.-E. Structure and properties of TiN coatings. *Thin Solid Film.* **1985**, *128*, 21–44. [[CrossRef](#)]
41. Chen, L.; Wang, S.Q.; Du, Y.; Li, J. Microstructure and mechanical properties of gradient Ti(C,N) and TiN/Ti(C,N) multilayer PVD coatings. *Mater. Sci. Eng. A.* **2007**, *478*, 336–339. [[CrossRef](#)]
42. Dobrzański, L.A.; Zukowska, L.W.; Mikuła, J.; Gołombek, K.; Pakuła, D.; Pancielejko, M. Structure and mechanical properties of gradient PVD coatings. *J. Mater. Process. Technol.* **2008**, *201*, 310–314. [[CrossRef](#)]
43. Yin, L.Y.; Zhang, J. Microstructure and mechanical properties of (TiAlNb)N films. *Adv. Mater. Res.* **2014**, *812*, 915–916. [[CrossRef](#)]
44. Polcar, T.; Cavaleiro, A. High-temperature tribological properties of CrAlN, CrAlSiN and AlCrSiN coatings. *Surf. Coat. Technol.* **2011**, *206*, 1244–1251. [[CrossRef](#)]
45. Kawate, M.; Hashimoto, A.K.; Suzuki, T. Oxidation Resistance of CrAlN and TiAlN Films. *Surf. Coat. Technol.* **2003**, *165*, 163–167. [[CrossRef](#)]
46. Endrino, J.L.; Fox-Rabinovich, G.S.; Gey, C. Hard AlTiN, AlCrN PVD Coatings for Machining of Austenitic Stainless Steel. *Surf. Coat. Technol.* **2006**, *200*, 6840–6845. [[CrossRef](#)]
47. Fox-Rabinovich, G.S.; Beake, B.D.; Endrino, J.L.; Veldhuis, S.C.; Parkinson, R.; Shuster, L.S.; Migranov, M.S. Effect of Mechanical Properties Measured at Room and Elevated Temperatures on the Wear Resistance of Cutting Tools with TiAlN and AlCrN Coatings. *Surf. Coat. Technol.* **2006**, *200*, 5738–5742. [[CrossRef](#)]
48. Jäger, N.; Meindlhumer, M.; Zitek, M.; Spor, S.; Hruby, H.; Nahif, F.; Julin, J.; Rosenthal, M.; Keckes, J.; Mitterer, C.; et al. Impact of Si on the high-temperature oxidation of AlCr(Si)N coatings. *J. Mater. Sci. Technol.* **2022**, *100*, 91–100. [[CrossRef](#)]

Disclaimer/Publisher’s Note: The statements, opinions and data contained in all publications are solely those of the individual author(s) and contributor(s) and not of MDPI and/or the editor(s). MDPI and/or the editor(s) disclaim responsibility for any injury to people or property resulting from any ideas, methods, instructions or products referred to in the content.